Structural dynamic problems in time domain under uncertainty: an interval finite element approach

Naijia Xiao

Department of Microbiology and Plant Biology, University of Oklahoma, Norman, OK 73019, USA Email: naijia.xiao@ou.edu

Francesco Fedele and Rafi L. Muhanna*

School of Civil and Environmental Engineering, Georgia Institute of Technology, Atlanta, GA 30332, USA

Email: fedele@gatech.edu Email: rafi.muhanna@gatech.edu

*Corresponding author

Abstract: An analysis of the structural dynamic response under uncertainty is presented. Uncertainties in load and material are modelled as intervals exploiting the interval finite element method (IFEM). To reduce overestimation and increase the computational efficiency of the solution, we do not solve the dynamic problem by an explicit step-by-step time integration scheme. Instead, our approach solves for the structural variables in the whole time domain simultaneously by an implicit scheme using discrete Fourier transform and its inverse (DFT and IDFT). Non-trivial initial conditions are handled by modifying the right-hand side of the governing equation. To further reduce overestimation, a new decomposition strategy is applied to the IFEM matrices, and both primary and derived quantities are solved simultaneously. The final solution is obtained using an iterative enclosure method, and in our numerical examples the exact solution is enclosed at minimal computational cost.

Keywords: interval finite element method; dynamic response; discrete Fourier transform; matrix decomposition; iterative enclosure method.

Reference to this paper should be made as follows: Xiao, N., Fedele, F. and Muhanna, R.L. (2018) 'Structural dynamic problems in time domain under uncertainty: an interval finite element approach', *Int. J. Reliability and Safety*, Vol. 12, Nos. 1/2, pp.122–146.

Biographical notes: Naijia Xiao received his PhD from Georgia Institute of Technology in the area of Computational structural mechanics. Currently he works at the Institute of Environmental Genetics, Department of Microbiology and Plant Biology, University of Oklahoma. His research interests include uncertainties in structural problems and network analysis.

Francesco Fedele is an Associate Professor in the School of Civil and Environmental Engineering and in the School of Electrical and Computer Engineering at Georgia Tech. He received his PhD in Civil Engineering from the University of Vermont in 2004 and earned his Laurea (magna cum laude) in Civil Engineering from the University Mediterranea, Italy, in 1998. His current research focus is on nonlinear wave phenomena, coastal and ocean engineering, fluid mechanics, wave mechanics, sustainable ocean energy, signal processing and computer vision, computational methods and inverse problems

Rafi L. Muhanna received his PhD in Computational Solid and Structural Mechanics from the Higher Institute for Structure and Architecture, Sofia, Bulgaria. He joined the Faculty of Damascus University, Syria in 1980 and Georgia Institute of Technology in 2000, where he founded the Center for Reliable Engineering Computing. His research activity is in the general area of computational solid and structural mechanics with focus on uncertainty modelling and structural reliability. He won a number of international prizes, among them: the Aga Khan Award for Architecture (1992); the Golden Prize of the World Intellectual Property Organization (WIPO), for the best-exposed patent at the International Fair of Damascus (1988); and the Special Prize of the United Nations HABITAT (1989). He is a member of the American Society of Civil Engineers and the American Society of Mechanical Engineers.

This paper is a revised and expanded version of a paper entitled 'Structural Dynamic Response under Uncertainty - An Interval Finite Element Approach' presented at REC2016, Bochum, Germany, 15–17 June 2016.

1 Introduction

In any physical system, uncertainties are inevitable when dealing with measurement devices and environmental conditions associated with a data acquisition process (Fernández-Martínez et al., 2013). Thus, it is necessary to model and track the propagation of uncertainties in the system and to reliably evaluate the accuracy of predicted system response. Conventional treatment of uncertainties uses probability theory (Lutes and Sarkani, 2004). The probability approach is preferred when measurements are abundant and sufficient to reliably predict the nature of the uncertainties. However, when measurements are scarce non-probabilistic approaches are preferred (Moens and Hanss, 2011; Zhang, 2005) such as Bayesian networks (Igusa et al., 2002; Soize, 2013; Unger and Könke, 2011), fuzzy sets (Adhikari and Khodaparast, 2014; Dehghan et al., 2006; Erdogan and Bakir, 2013; Klir and Wierman, 1999), evidence theory (Bai et al., 2013; Dempster, 1967; Jiang et al., 2013; Shafer, 1968), and intervals (Corliss et al., 2007; Do et al., 2014; Impollonia and Muscolino, 2011; Muhanna et al., 2007).

In this work, we adopt the interval approach modelling uncertainties by way of interval numbers with their respective lower and upper bounds. For the mathematical foundation of interval arithmetic we refer the reader to Alefeld and Herzberger (1984), Kulisch and Miranker (1981), and Moore et al. (2009).

The interval-based approach will be exploited for the analysis of structural dynamic problems in the time domain under uncertainty. In particular, we study the dynamics of elastic structures with uncertain load, geometric and material properties. Uncertain structural parameters are modelled by intervals, and the system response is evaluated by means of the Interval Finite Element Method (IFEM) (Hu and Qiu, 2010; Qiu and Ni,

2010; To, 2012; Xia et al., 2010). From now on, non-italic **bold** letters are used to denote interval variables. The dynamical response of a structure with uncertain parameters is governed by the following interval differential equation

$$\mathbf{K}\mathbf{u} + \mathbf{D}\dot{\mathbf{u}} + \mathbf{M}\ddot{\mathbf{u}} = \mathbf{f},\tag{1}$$

where the interval matrices K, D, and M are respectively the stiffness, damping, and mass matrix of the structure, u is the unknown interval nodal displacement vector, \dot{u} and \ddot{u} are the corresponding interval nodal velocity and acceleration vector, f is the time-varying interval nodal equivalent load. The uncertain initial conditions are expressed in the interval form

$$\mathbf{u}(0) = \mathbf{u}_0, \qquad \dot{\mathbf{u}}(0) = \mathbf{v}_0, \tag{2}$$

where \mathbf{u}_0 and \mathbf{v}_0 are the initial nodal displacement and velocity vector, respectively.

In practice, the differential equation (1) is solved at discrete times t_k uniformly spaced in time. Conventional numerical integration approaches, such as the Newmark- β method (De Borst et al., 2012; Dokainish and Subbaraj, 1989; Paz, 1997), solve for equation (1) recursively, viz. the solution at the current time t_k depends on the solution at the previous time t_{k-1} . However, a straightforward generalisation of such recursive approaches to intervals yield overestimation due to the interval dependency between successive times. This accumulates at each time step leading to an interval enclosure of the solution that quickly becomes excessively wide after few iterations in time.

To reduce overestimation, we solve for the dynamical equations in the spectral domain (Bae et al., 2014; Yang et al., 2012) using the Discrete Fourier Transform (DFT) (Santamarina and Fratta, 2005). In particular, equation (1) is first transformed into the frequency domain using the DFT. The spectral response is then computed via intervals and transformed back into the time domain by way of the Inverse Discrete Fourier Transform (IDFT). As a result, the solution is as if solved simultaneously at all the time steps.

The paper is structured as follows. First, we present a short background on the formulation of IFEM including the new matrix decomposition strategy followed by the deterministic solver based on the DFT approach. Then the associated interval solver is introduced. The dynamical equation (1) is rewritten in a fixed-point form, and an iterative approach is adopted to obtain a sharp interval enclosure of the exact solution. Finally, the performance of the current method is compared against other available methods by way of several numerical examples.

2 Interval finite element formulation

The different formulations of conventional finite element methods in linear elastic systems lead to a linear system equations. When uncertainties are considered in the load and material/geometric properties in the form of intervals the formulation results in the IFEM, which is expressed in an interval linear system of equations whose coefficients are intervals that appear in the system matrices, for example, in the static linear case, the structural equilibrium equation can be described by the following interval linear system

$$\mathbf{K}\mathbf{u} = \mathbf{f},\tag{3}$$

where \mathbf{K} is the interval stiffness matrix, \mathbf{u} is the interval nodal displacement vector, and f is the interval nodal equivalent load vector. Then the proposed solver aims to obtain guaranteed interval enclosures for the primary unknown variable \mathbf{u} . The main challenge is the reduction of overestimation in the interval system solution due to interval dependency. The adopted strategy for overestimation reduction is matrix decomposition. While matrix decomposition is well known in mathematical formulations, however it is new in the context of reducing interval overestimation with the goal of obtaining sharp enclosures in the development of interval finite element methods. A detailed formulation of IFEM based on Element-By-Element and Lagrange multiplier approach is introduced in the previous work of the authors (Xiao, 2015; Rama Rao et al., 2011). Our focus in this work is the system matrices decomposition and its implementations in dynamic problems. To minimise overestimation we propose new matrix decomposition strategies that avoid multiple occurrences of the same interval variables, as a result overestimation due to interval dependency is reduced (Moore et al., 2009). For the sake of clarity and to provide a background for this strategy, we will illustrate the matrix decomposition in the linear static case and later in the paper will be extended to the dynamic case and discussed in details in Section 4. In particular, the interval stiffness matrix K and the interval nodal equivalent load f are decomposed into

$$\mathbf{K} = A \operatorname{diag}(\Lambda \boldsymbol{\alpha}) A^{T}, \quad \mathbf{f} = F \boldsymbol{\delta}, \tag{4}$$

where A, Λ , F are deterministic matrices, α is the interval stiffness parameter vector that accounts for the geometric and material uncertainties in K, and δ is the interval load uncertainty vector that accounts for the load uncertainty in f.

Note that matrix decomposition in equation (4) is performed at the element level before assembly. First, the element stiffness matrix \mathbf{K}_e and the element nodal equivalent load vector \mathbf{f}_e are computed. Their decomposition yields the element matrices A_e , Λ_e , F_e , α_e and δ_e . These are further assembled into their global counterparts A, Λ , F, α and δ . During the assembly, either the Element-by-Element (EBE) assembly strategy or the conventional strategy can be adopted (Xiao, 2015). In the following subsections, details on the aforementioned decompositions are discussed.

2.1 Element matrix decomposition

In this subsection, we present the matrix decomposition strategy applied to the interval element stiffness matrix \mathbf{K}_e and the element interval nodal equivalent load \mathbf{f}_e .

2.1.1 Decomposition of \mathbf{K}_{e}

According to equation (4), the element stiffness matrix \mathbf{K}_e is decomposed into

$$\mathbf{K}_{e} = A_{e} \operatorname{diag}(\Lambda_{e} \boldsymbol{\alpha}_{e}) A_{e}^{T}, \tag{5}$$

where A_e and Λ_e are deterministic matrices, and α_e accounts for the geometric and material uncertainties in \mathbf{K}_e . In the following discussion, plane truss, plane frame, and plane stress/strain elements are presented, however the formulation has a general nature and can be implemented for other finite elements.

126

First, we introduce the standard two-node plane truss-bar element. Since the geometry and material properties are affected by uncertainties, we model the cross section area $\bf A$ and the Young's modulus $\bf E$ as intervals. The corresponding element interval stiffness matrix $\bf K_e$ in the local coordinate system is given by

$$\mathbf{K}_{e} = \begin{cases} \frac{\mathbf{E}\mathbf{A}}{L} & 0 & -\frac{\mathbf{E}\mathbf{A}}{L} & 0\\ 0 & 0 & 0 & 0\\ -\frac{\mathbf{E}\mathbf{A}}{L} & 0 & \frac{\mathbf{E}\mathbf{A}}{L} & 0\\ 0 & 0 & 0 & 0 \end{cases}$$
 (6)

where L is the element length. The above element stiffness matrix is decomposed into the following elementary matrices:

$$A_e = \{-1 \quad 0 \quad 1 \quad 0\}^T, \qquad \Lambda_e = \{1/L\}, \qquad \boldsymbol{\alpha}_e = \{\mathbf{E}\mathbf{A}\}, \tag{7}$$

where α_e contains the only interval variables **EA** in the element, and the corresponding deterministic matrices are A_e and Λ_e .

For the standard two-node Euler-Bernoulli beam elements, the uncertain parameters; the cross section area A, the moment of inertia I, and the Young's modulus E are modelled as intervals. Considering the axial and bending deformation, the corresponding K_e in the local coordinate system is given by

$$\mathbf{K}_{e} = \begin{cases}
\frac{\mathbf{E}\mathbf{A}}{L} & 0 & 0 & -\frac{\mathbf{E}\mathbf{A}}{L} & 0 & 0 \\
0 & \frac{12\mathbf{E}\mathbf{I}}{L^{3}} & \frac{6\mathbf{E}\mathbf{I}}{L^{2}} & 0 & -\frac{12\mathbf{E}\mathbf{I}}{L^{3}} & \frac{6\mathbf{E}\mathbf{I}}{L^{2}} \\
0 & \frac{6\mathbf{E}\mathbf{I}}{L^{2}} & \frac{4\mathbf{E}\mathbf{I}}{L} & 0 & -\frac{6\mathbf{E}\mathbf{I}}{L^{2}} & \frac{2\mathbf{E}\mathbf{I}}{L} \\
-\frac{\mathbf{E}\mathbf{A}}{L} & 0 & 0 & \frac{\mathbf{E}\mathbf{A}}{L} & 0 & 0 \\
0 & -\frac{12\mathbf{E}\mathbf{I}}{L^{3}} & -\frac{6\mathbf{E}\mathbf{I}}{L^{2}} & 0 & \frac{12\mathbf{E}\mathbf{I}}{L^{3}} & -\frac{6\mathbf{E}\mathbf{I}}{L^{2}} \\
0 & \frac{6\mathbf{E}\mathbf{I}}{L^{2}} & \frac{2\mathbf{E}\mathbf{I}}{L} & 0 & -\frac{6\mathbf{E}\mathbf{I}}{L^{2}} & \frac{4\mathbf{E}\mathbf{I}}{L}
\end{cases}$$
(8)

where L is the element length. Then α_e contains the element axial stiffness **EA** and the element bending stiffness **EI**. The corresponding A_e is a 6×3 matrix, whose columns are the eigenvectors of \mathbf{K}_e , and Λ_e is a 3×2 matrix, are

$$A_{e} = \begin{cases} 1 & 0 & 0 \\ 0 & 0 & 2 \\ 0 & 1 & L \\ -1 & 0 & 0 \\ 0 & 0 & -2 \\ 0 & -1 & L \end{cases}, \quad \Lambda_{e} = \begin{cases} \frac{1}{L} & 0 \\ 0 & \frac{1}{L} \\ 0 & \frac{3}{L^{3}} \end{cases}, \quad \boldsymbol{\alpha}_{e} = \begin{cases} \mathbf{E}\mathbf{A} \\ \mathbf{E}\mathbf{I} \end{cases}.$$
(9)

Note that the matrix decomposition strategy that lead to equations (7) and (9) is not unique. Indeed, this approach requires analytic expressions for \mathbf{K}_e , which are usually not available for the general types of finite elements. A more general approach regardless the finite element type is based on numerical integration. As an example, we consider plane stress/strain elements.

For standard 8-node rectangular isoparametric elements in plane stress/strain problem, the element Young's modulus \mathbf{E} is modelled as intervals. Then the corresponding \mathbf{K}_e is given by

$$\mathbf{K}_{e} = \int_{\Omega} B_{e}^{T}(\xi) \mathbf{E}_{e}(\xi) B_{e}(\xi) t(\xi) d\Omega, \tag{10}$$

where the integration domain Ω is the entire element, t is the thickness, and B_e is the strain-displacement matrix. For isotropic material with Poisson's ratio ν , the interval constitutive matrix \mathbf{E}_e for plane stress state is given by

$$\mathbf{E}_{e} = \frac{\mathbf{E}}{1 - v^{2}} \begin{cases} 1 & v & 0 \\ v & 1 & 0 \\ 0 & 0 & \frac{1 - v}{2} \end{cases}. \tag{11}$$

and for plane strain state,

$$\mathbf{E}_{e} = \frac{\mathbf{E}}{(1 - 2\nu)(1 + \nu)} \begin{cases} 1 - \nu & \nu & 0 \\ \nu & 1 - \nu & 0 \\ 0 & 0 & \frac{1 - 2\nu}{2} \end{cases}$$
 (12)

The double integral in equation (10) can be evaluated numerically by using a 3×3 Gaussian integration rule, that is

$$\mathbf{K}_{e} = \sum_{j=1}^{9} B_{e}^{T}(\xi_{j}) \mathbf{E}_{e}(\xi_{j}) B_{e}(\xi_{j}) w_{j} J(\xi_{j}) t(\xi_{j}), \tag{13}$$

where the coordinates ξ_j and weights w_j for all the integration points in the standard domain $[-1,1]\times[-1,1]$ are given, and J is the determinant of the Jacobian of the coordinate transformation between the local and global coordinate system. Note that the use of numerical integration has the effect of changing the modulus from a spatial function bounded by interval values to a function described by interval coefficients. Thus the discretisation by the finite element methods results in additional smoothness in the spatial variation of the modulus field.

In equation (13), the only interval term \mathbf{E} can be factored out, viz. $\mathbf{K}_e = P_e \mathbf{E}$, where P_e is a deterministic matrix. This can be decomposed as $P_e = A_e diag(\Lambda_e) A_e^T$, where Λ_e is the eigenvalue matrix and the columns of A_e are the corresponding eigenvectors. Note

that Λ_e includes three zero eigenvalues, which correspond to rigid body motion of two translations and one rotation. They are dropped and equation (13) is rewritten as

$$\mathbf{K}_{e} = A_{e} \operatorname{diag}(\Lambda_{e}) A_{e}^{T} \boldsymbol{\alpha}_{e} = A_{e} \operatorname{diag}(\Lambda_{e} \boldsymbol{\alpha}_{e}) A_{e}^{T}, \tag{14}$$

where $\alpha_e = \{E\}$ is the only interval quantity. One can also use an LDL decomposition of P_e . As a result, A_e is a lower triangular matrix, and Λ_e is also different.

In the above decomposition strategy, P_e is explicitly computed in order to obtain A_e and Λ_e . In addition, the Young's modulus \mathbf{E} is assumed to be constant inside the element. Alternatively, the B-matrix approach (Xiao, 2015) can be adopted, in which P_e is never explicitly computed and the element stiffness parameter vector $\boldsymbol{\alpha}_e$ contains \mathbf{E}_j at all the numerical integration points.

Finally, note that the decomposition of diagonal matrix $\operatorname{diag}(\Lambda_e \alpha_e)$ is novel in the current method, when compared with others in the literature (Gao, 2007; Impollonia, 2006; Neumaier and Pownuk, 2007). The decomposition reduces multiple occurrences of interval terms to the minimum. In later discussions on iterative enclosure method, this decomposition plays an important role.

2.1.2 Decomposition of f

The element nodal equivalent load vector \mathbf{f}_e is decomposed into the following form using the $M - \delta$ method (Mullen and Muhanna, 1999),

$$\mathbf{f}_{o} = F_{o} \boldsymbol{\delta}_{o}. \tag{15}$$

Thus the interval terms in the element load uncertainty vector $\boldsymbol{\delta}_e$ is completely separated from the deterministic part F_e of the equivalent load. For an arbitrary element, the nodal equivalent load vector is given by

$$\mathbf{f}_{e} = \sum_{j} N^{T}(\xi_{j}) \mathbf{f}_{0}(\xi_{j}) + \int_{\Omega_{1}} N^{T}(\xi) \mathbf{f}_{1}(\xi) d\Omega_{1} + \int_{\Omega_{2}} N^{T}(\xi) \mathbf{f}_{2}(\xi) d\Omega_{2} + \int_{\Omega_{3}} N^{T}(\xi) \mathbf{f}_{3}(\xi) d\Omega_{3},$$

$$(16)$$

where $N(\xi)$ is the shape function matrix, ξ is the local coordinate of the element, ξ_j are coordinates where concentrated load is applied, $\mathbf{f}_0(\xi_j)$ are the concentrated loads under consideration, Ω_1 , Ω_2 , Ω_3 are the integration domains in which line load \mathbf{f}_1 , surface load \mathbf{f}_2 , volume load \mathbf{f}_3 are non-zero.

By rewriting $\mathbf{f}_j(\xi) = L_j(\xi) \boldsymbol{\delta}_e$ (j = 0,1,2,3), the interval element load uncertainty vector $\boldsymbol{\delta}_e$ can be separated from the deterministic part of \mathbf{f}_e . Then

$$F_{e} = \sum_{j} N^{T}(\xi_{j}) L_{0}(\xi_{j}) + \int_{\Omega_{1}} N^{T}(\xi) L_{1}(\xi) d\Omega_{1} + \int_{\Omega_{2}} N^{T}(\xi) L_{2}(\xi) d\Omega_{2} + \int_{\Omega_{3}} N^{T}(\xi) L_{3}(\xi) d\Omega_{3},$$
(17)

As a first example, consider the Euler-Bernoulli beam element of length L shown in Figure 1. The element is subject to concentrated loads \mathbf{p}_c and \mathbf{q}_c applied at distance a

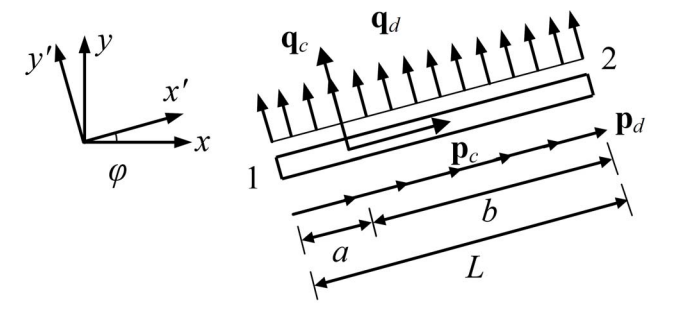
from node 1, as well as transverse uniform load \mathbf{q}_d and axial uniform load \mathbf{p}_d along the element. Then the element nodal equivalent load vector \mathbf{f}_e and its decomposition are given by

$$\mathbf{f} = \begin{cases} \frac{b}{L} \mathbf{p}_{c} + \frac{L}{2} \mathbf{p}_{d} \\ \frac{b}{L} \mathbf{q}_{c} + \frac{L}{2} \mathbf{q}_{d} \\ \frac{L^{2}}{12} \mathbf{q}_{d} \\ \frac{a}{L} \mathbf{p}_{c} + \frac{L}{2} \mathbf{p}_{d} \\ \frac{a}{L} \mathbf{q}_{c} + \frac{L}{2} \mathbf{q}_{d} \\ \frac{L^{2}}{12} \mathbf{q}_{d} \end{cases} = \begin{cases} \frac{b}{L} & 0 & \frac{L}{2} & 0 \\ 0 & \frac{b}{L} & 0 & \frac{L}{2} \\ 0 & 0 & 0 & \frac{L^{2}}{12} \\ 0 & \frac{a}{L} & 0 & \frac{L}{2} \\ 0 & 0 & 0 & \frac{L^{2}}{12} \end{cases} \begin{cases} \mathbf{p}_{c} \\ \mathbf{q}_{c} \\ \mathbf{p}_{d} \\ \mathbf{q}_{d} \end{cases} = F_{e} \delta_{e},$$

$$(18)$$

where the load uncertainty vector $\boldsymbol{\delta}_e$ contains the four intervals in \mathbf{f}_e , and each column of F_e corresponds to one of them.

Figure 1 Distributed and concentrated loads acting on a two-node Euler-Bernoulli beam element

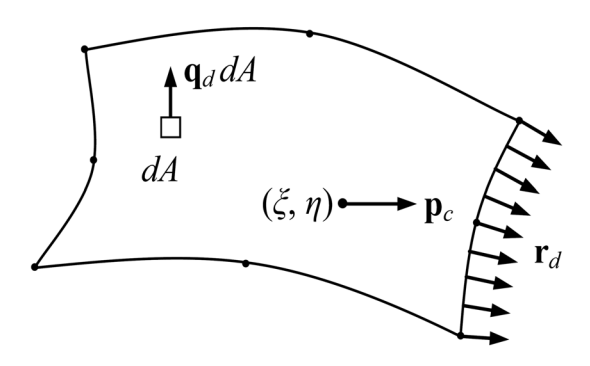


As a second example, consider the 8-node rectangular isoparametric element in Figure 2. The element is subject to a concentrated load \mathbf{p}_c in the x-direction at (ξ, η) , a uniform body load \mathbf{q}_d in the y-direction, and a uniform line load \mathbf{r}_d outwards on the right edge. Then $\boldsymbol{\delta}_e = \{\mathbf{p}_c \ \mathbf{q}_d \ \mathbf{r}_d\}^T$ and F_e is given by

$$F_{e} = \begin{cases} N_{1}(\xi, \eta) & 0 & \int_{x=0}^{L} N_{1}J_{11}dl \\ 0 & \iint_{A} N_{1}(\xi, \eta)dA & \int_{x=0}^{L} N_{1}J_{21}dl \\ \vdots & \vdots & \vdots \\ N_{8}(\xi, \eta) & 0 & \int_{x=0}^{L} N_{8}J_{11}dl \\ 0 & \iint_{A} N_{8}(\xi, \eta)dA & \int_{x=0}^{L} N_{8}J_{21}dl \end{cases},$$
(19)

where N_j is the shape function with respect to the *j*-th node, L is the length of the right edge, and $\{J_{11} J_{21}\}^T$ is the first column of the Jacobian, accounting for the uniform load \mathbf{r}_d acting on the right edge. The formulation can be easily extended to cases when the loads are non-uniform or defined in the local coordinate system.

Figure 2 Concentrated, body and line loads acting on an 8-node rectangular isoparametric element



2.2 Element assembly strategies

In this subsection, \mathbf{K}_e , \mathbf{f}_e , and B_e are assembled into their global counterparts \mathbf{K} , \mathbf{f} , and B. At the same time, the assembly rules for the decomposed matrices are presented. Two assembly strategies are introduced here: one is the Element-by-Element approach, which assembles the matrices block-by-block; the other is the conventional FEM assembly strategy (Xiao, 2015).

2.2.1 Element-by-Element assembly

In the Element-by-Element approach, the structure is modelled by separated elements and common nodes that connect the elements. As a result, the structural nodal displacement vector \mathbf{u} is a collection of all the element nodal displacement vectors \mathbf{u}_e , and the nodal displacement vector \mathbf{u}_n of the common nodes. Then the global stiffness matrix \mathbf{K} and nodal equivalent load \mathbf{f} are assembled from their element counterparts

$$\mathbf{u} = \begin{cases} \mathbf{u}_{e} \\ \vdots \\ \mathbf{u}_{e} \\ \mathbf{u}_{n} \end{cases}, \quad \mathbf{K} = \begin{cases} \mathbf{K}_{e} \\ \vdots \\ \mathbf{K}_{e} \\ 0 \end{cases}, \quad \mathbf{f} = \begin{cases} \mathbf{f}_{e} \\ \vdots \\ \mathbf{f}_{e} \\ \mathbf{f}_{n} \end{cases}, \tag{20}$$

where \mathbf{f}_n denotes concentrated forces applied directly on the common nodes. In contrast to the standard FEM assembly, \mathbf{K} and \mathbf{f} are assembled block by block from the individual element stiffness \mathbf{K}_e and individual element load \mathbf{f}_e , respectively (Rama Rao et al., 2011). Note that \mathbf{K} is a singular matrix.

To reduce overestimation due to dependency of multiple occurrences of the same variable, **K** and **f** are further decomposed, that is, $\mathbf{K} = Adiag(\Lambda \boldsymbol{\alpha})A^T$ and $\mathbf{f} = F\boldsymbol{\delta}$. The element vectors $\boldsymbol{\alpha}_e$ and $\boldsymbol{\delta}_e$ can be selected components of the global interval vectors $\boldsymbol{\alpha}$ and $\boldsymbol{\delta}$, or they can be interpolated from $\boldsymbol{\alpha}$ and $\boldsymbol{\delta}$. In either way, they can be brought into the following form,

$$\boldsymbol{\alpha}_{e} = L_{\alpha} \boldsymbol{\alpha}, \quad \boldsymbol{\delta}_{e} = L_{\delta} \boldsymbol{\delta}.$$
 (21)

The corresponding assembly rule for A, Λ , and F is quite similar to the assembly rule for \mathbf{K} and \mathbf{f} . Indeed, they are all assembled block by block,

$$A = \begin{cases} A_e & & \\ & \ddots & \\ & & A_e \\ 0 & \cdots & 0 \end{cases}, \quad \Lambda = \begin{cases} \Lambda_e L_\alpha \\ \vdots \\ \Lambda_e L_\alpha \end{cases}, \quad F = \begin{cases} F_e L_\delta \\ \vdots \\ F_e L_\delta \\ F_n \end{cases}. \tag{22}$$

where $\mathbf{f}_n = F_n \boldsymbol{\delta}$ is the decomposition of \mathbf{f}_n . In the derivation, it is assumed that each interval component in $\boldsymbol{\alpha}$ and $\boldsymbol{\delta}$ varies independently. If two or more components in $\boldsymbol{\alpha}$ or $\boldsymbol{\delta}$ represent the same variable, corresponding columns in $\boldsymbol{\Lambda}$ or F should be added together. If certain entries in $\boldsymbol{\delta}$ were equal to zero, the corresponding columns in F should be deleted. To impose compatibility and equilibrium, Lagrangian multiplier $\boldsymbol{\lambda}$ is introduced to enforce the constraint $C\mathbf{u} = 0$. The energy functional $\boldsymbol{\Pi}$ of the system is

$$\Pi = \frac{1}{2} \mathbf{u}^T \mathbf{K} \mathbf{u} - \mathbf{u}^T \mathbf{f} + \boldsymbol{\lambda}^T C \mathbf{u}.$$
 (23)

Minimising Π with respect to **u** and λ yields the interval governing equations

$$\begin{cases}
\mathbf{K} & C^T \setminus \mathbf{u} \\
C & 0 \quad \lambda
\end{cases} =
\begin{cases}
\mathbf{f} \\
0
\end{cases}.$$
(24)

To reduce overestimation, **K** and **f** are decomposed as in equation (4) Thus

$$\begin{pmatrix} A \\ 0 \end{pmatrix} diag(\Lambda \Delta \boldsymbol{\alpha}) \{A^T \ 0\} + \begin{cases} K_0 & C^T \\ C & 0 \end{cases} \} \begin{pmatrix} \mathbf{u} \\ \boldsymbol{\lambda} \end{pmatrix} = \begin{cases} F \\ 0 \end{cases} \boldsymbol{\delta}, \tag{25}$$

where $\Delta \boldsymbol{\alpha}$ is the difference between interval vector $\boldsymbol{\alpha}$ and its reference vector α_0 , viz. $\Delta \boldsymbol{\alpha} = \boldsymbol{\alpha} - \alpha_0$, and $K_0 = Adiag(\Lambda \alpha_0)A^T$. Preferably, $\alpha_0 = mid \boldsymbol{\alpha}$.

The Lagrangian multiplier λ denotes negative internal forces between element nodes and common nodes when the constraint is a compatibility condition and λ denotes reactions at the supports when the constraint is an essential boundary condition. Thus internal forces and support reactions are obtained as a by-product as the Lagrangian multiplier λ enforcing the constraint equation $C\mathbf{u}=0$.

2.2.2 Conventional assembly

The conventional assembly strategy provides smaller stiffness matrix and is more efficient for large scale problems. In this case, the global nodal displacement vector \mathbf{u} contains only displacement vector \mathbf{u}_n of the common nodes. The global stiffness matrix and nodal equivalent load vector are given by

$$\mathbf{K} = \sum_{e} T_{e}^{T} \mathbf{K}_{e} T_{e}, \qquad \mathbf{f} = \sum_{e} T_{e}^{T} \mathbf{f}_{e} + \mathbf{f}_{n}, \tag{26}$$

where T_e is the transformation matrix between the global and local nodal displacement vector \mathbf{u} and \mathbf{u}_e . By inserting $\mathbf{K}_e = A_e diag(\Lambda_e \boldsymbol{\alpha}_e) A_e^T$ into equation (26), the decomposition rule for \mathbf{K} follows as

$$\mathbf{K} = \sum_{e} T_{e}^{T} A_{e} diag(\Lambda_{e} \boldsymbol{\alpha}_{e}) A_{e}^{T} T_{e}$$

$$= \left\{ T_{e}^{T} A_{e} \dots T_{e}^{T} A_{e} \right\} diag \begin{cases} \Lambda_{e} \boldsymbol{\alpha}_{e} \\ \vdots \\ \Lambda_{e} \boldsymbol{\alpha}_{e} \end{cases} \begin{cases} A_{e}^{T} T_{e} \\ \vdots \\ A_{e}^{T} T_{e} \end{cases}.$$

$$(27)$$

The assembly rules for A and Λ are given by

$$A = T_e^T A_e \dots T_e^T A_e, \qquad \Lambda = \begin{cases} \Lambda_e L_\alpha \\ \vdots \\ \Lambda_e L_\alpha \end{cases}. \tag{28}$$

Similarly, using the decompositions $\mathbf{f}_e = F_e \boldsymbol{\delta}_e$ and $\mathbf{f}_n = F_n \boldsymbol{\delta}_n$, the nodal equivalent load \mathbf{f} in equation (26) can be written as

$$\mathbf{f} = \sum_{e} T_e^T F_e \boldsymbol{\delta}_e + F_n \boldsymbol{\delta}_n. \tag{29}$$

The assembly rule for F is given by

$$F = \sum_{e} T_e^T F_e L_{\delta} + F_n. \tag{30}$$

After assembling all matrices, the energy functional in equation (23) is formulated and minimised with respect to \mathbf{u} and λ which will yield the same form of interval governing equations (24) and (25) but with a different structure of matrices that is consistent with the assembly.

3 Deterministic dynamic solver

In this section, the deterministic dynamic solver based on the DFT (Veletsos and Kumar, 1983; Veletsos and Ventura, 1985) is presented. The FEM equations to solve for the dynamic response of a linearly elastic structure are given by

$$Ku + D\dot{u} + M\ddot{u} = f, (31)$$

where K, D, and M are the stiffness, damping, and mass matrices of the structure, respectively, u is the nodal displacement vector, \dot{u} and \ddot{u} are the first and second derivatives of u with respect to the time (or, equivalently, nodal velocity and acceleration), and f is the nodal equivalent load. The initial conditions are given by

$$u(0) = u_0, \qquad \dot{u}(0) = v_0.$$
 (32)

To impose compatibility and equilibrium, Lagrangian multiplier λ is introduced to enforce the constraint $C\mathbf{u} = 0$. The energy functional Π of the system is

$$\mathbf{\Pi} = \frac{1}{2} \mathbf{u}^T \mathbf{K} \mathbf{u} - \mathbf{u}^T \mathbf{f} + \boldsymbol{\lambda}^T C \mathbf{u}.$$
 (33)

Minimising Π with respect to **u** and λ yields the interval governing equations

$$\begin{cases}
\mathbf{K} & C^T \\
C & 0
\end{cases}
\begin{cases}
\mathbf{u} \\
\lambda
\end{cases} =
\begin{cases}
\mathbf{f} \\
0
\end{cases}.$$
(34)

The dynamics is solved over a given time interval, which is discretised into uniformly spaced times t_k . The nodal equivalent load at the discrete time t_k is known, and we want to solve for the nodal displacement vector u at t_k and its time derivatives \dot{u} and \ddot{u} , viz. velocity and acceleration respectively. That is, $f(t_k) = f_k$, $u(t_k) = u_k$, $\dot{u}(t_k) = \dot{u}_k$. We assume that time steps are uniformly spaced, viz. $t_k = k\Delta t$. The sampling interval Δt must be small enough to prevent any potential aliasing (Santamarina and Fratta, 2005). Let T be the total time length of the signal and N the number of time steps Δt in the total time length, then $T = N\Delta t$.

The governing equation (31) is transformed in the spectral domain via the DFT into

$$\left(-\omega_{i}^{2}M + i\omega_{i}D + K\right)\mathcal{F}_{t}(u)_{i} = \mathcal{F}_{t}(f)_{i}, \tag{35}$$

or

$$K_{DS}\mathcal{F}_{t}(u)_{i} = \mathcal{F}_{t}(f)_{i}, \tag{36}$$

where K_{DS} is the dynamic stiffness, $i = \sqrt{-1}$ is the imaginary unit, $\omega_j = j\Delta\omega$ with $\Delta\omega = 2\pi/T$ being the fundamental frequency, $\mathcal{F}_t(u)_j$ and $\mathcal{F}_t(f)_j$ are the Fourier transform of the nodal displacement u_k and equivalent load f_k , respectively. Then the nodal displacement vector in the time-domain is obtained by applying the IDFT to $\mathcal{F}_t(u)_j$, viz.

$$u_{n} = \frac{1}{N} \sum_{i=0}^{N-1} \mathcal{F}_{t}(u)_{j} e^{-i(2\pi/N)jn} = \frac{1}{N} \sum_{i=0}^{N-1} G_{j} \mathcal{F}_{t}(f)_{j} e^{-i(2\pi/N)jn},$$
(37)

where G_j is the inverse of the dynamic stiffness matrix in equation (36). To ensure that the final solution u_n is real, i.e., null imaginary part, G_j takes the following form,

$$G_{j} = \begin{cases} \left(-\omega_{j}^{2} M + i\omega_{j} D + K\right)^{-1}, & 0 \le j < N/2; \\ conjugate of G_{N-j}, & N/2 \le j < N. \end{cases}$$
(38)

The above approach essentially solves for the stationary response of the structure caused by periodic loads with period T. The results are identical to the actual dynamic response with trivial initial conditions ($u_0 = v_0 = 0$) when zero-padding is applied. The length of the zero-padding, T_p , can be estimated from

$$e^{-\zeta\omega T_p} < \tau_{err}, \quad \Rightarrow \quad T_p > \frac{\ln \tau_{err}}{\zeta\omega},$$
 (39)

where τ_{err} is the error tolerance, ω is the lowest natural frequency of the structure, and ζ is the corresponding effective damping ratio. Let T_0 be the length of the original signal, then $T = T_0 + T_p$.

Non-trivial initial conditions can be modelled by modifying the equivalent load (Lee et al., 2005; Liu et al., 2015, Mansur et al., 2000). For initial displacement u_0 , it is equivalent to add a constant load $f_{u0} = Ku_0$, which exist for the time interval $T_0 \le t < T$. For initial velocity v_0 , it is equivalent to add an impulse load $f_{v0} = Mv_0 / \Delta t$, at time t = 0 for a duration of time Δt .

4 Interval dynamic solver

Consider an elastic structure characterised by uncertain parameters of the load, material, and geometry, which are modelled by intervals. The structural system is governed by equations (1) and (2). For simplicity, the Rayleigh damping is adopted. The damping matrix

$$\mathbf{D} = \alpha_{d} \mathbf{M} + \beta_{d} \mathbf{K},\tag{40}$$

where α_d and β_d are the Rayleigh damping coefficients. To reduce overestimation due to interval dependency, the interval matrix decomposition outlined in section 2 is adopted. Then DFT is used to transform the governing equation into a fixed-point form, which is further solved by a new variant of iterative enclosure method. Details on the current method are presented in the following subsections.

4.1 Interval matrix decomposition

Following the matrix decomposition strategy introduced in section 2, the overestimation reduction due to interval dependency is achieved by avoiding multiple occurrences of the same interval variable in the IFEM formulation. The stiffness matrix \mathbf{K} , and the mass matrix \mathbf{M} are decomposed into

$$\mathbf{K} = A \operatorname{diag}(\Lambda \boldsymbol{\alpha}) A^{T}, \qquad \mathbf{M} = A_{\mathbf{m}} \operatorname{diag}(\Lambda_{\mathbf{m}} \boldsymbol{\alpha}_{\mathbf{m}}) A_{\mathbf{m}}^{T}, \tag{41}$$

where A, A_m , Λ , and Λ_m are deterministic matrices, α is the interval stiffness parameter vector that accounts for uncertainties in the stiffness matrix \mathbf{K} , and α_m is the interval mass parameter vector that accounts for uncertainties in the mass matrix \mathbf{M} . Details about the implementation of this decomposition are introduced in the authors' previous work (Xiao, 2015).

By combining the nodal equivalent load vector \mathbf{f}_k at different time steps t_k , the interval load matrix \mathbf{f} is obtained, whose k-th column is \mathbf{f}_k . When the structure is subject to external loading and the M- δ method is adopted (Muhanna and Mullen 2001), \mathbf{f} is decomposed into

$$\mathbf{f} = F\boldsymbol{\delta}_{t},\tag{42}$$

where F is a deterministic matrix, and $\boldsymbol{\delta}_t$ is the time-varying load uncertainty matrix. Usually it is necessary to distinguish the uncertainty in the magnitude of the load and the uncertainty in the time-history of the load. Thus $\boldsymbol{\delta}_t$ is further decomposed into an interval column vector $\boldsymbol{\delta}$ and an interval row vector \mathbf{d}_t , viz. $\boldsymbol{\delta}_t = \boldsymbol{\delta} \mathbf{d}_t$, where $\boldsymbol{\delta}$ models the uncertainties in the load magnitude and \mathbf{d}_t models the uncertainties in the load time-history. Finally, the nodal equivalent load \mathbf{f} is decomposed into

$$\mathbf{f} = (F\boldsymbol{\delta})\mathbf{d}_{t}. \tag{43}$$

Similarly, when the structure is subject to ground motion, f is decomposed into

$$\mathbf{f} = -\mathbf{M}\mathbf{a} = -\mathbf{M}q\boldsymbol{\delta}_{t},\tag{44}$$

where δ_t denotes the time-varying ground acceleration, **a** represents the resulting nodal acceleration of the structure, and q relates δ_t to **a**, viz. $\mathbf{a} = q\delta_t$. By using the same decomposition for δ_t , and noting equation (41),

$$\mathbf{f} = -A_m \operatorname{diag}(\Lambda_m \boldsymbol{\alpha}_m) A_m^T q \boldsymbol{\delta} \mathbf{d}_t = A_m \left(\Lambda_m \boldsymbol{\alpha}_m \circ \boldsymbol{B}_t \boldsymbol{\delta}\right) \mathbf{d}_t, \tag{45}$$

where $B_f = -A_m^T q$, and $a \circ b$ is the element-by-element Hadamard product of two vectors a and b.

When the initial conditions are non-trivial and modelled by intervals, as shown in equation (2), the corresponding nodal equivalent load \mathbf{f} is given by

$$\mathbf{f} = \mathbf{K}\mathbf{u}_0 d_{u_0} + \mathbf{M}\mathbf{v}_0 d_{v_0}, \tag{46}$$

where d_{u_0} and d_{v_0} are two deterministic row vectors. The value of d_{u_0} is zero for the time interval $0 \le t_k < T_0$ and unity for the time interval $T_0 \le t_k < T$, where T_0 and T are the length of the original and padded signal and d_{u_0} represents an impulse load which has the value $1/\Delta t$ at $t_k = 0$ and zero everywhere else. Noting the decomposition in equation (41),

$$\mathbf{f} = A(\Lambda \boldsymbol{\alpha} \circ A^T \mathbf{u}_0) d_{u_0} + A_m (\Lambda_m \boldsymbol{\alpha}_m \circ A_m^T \mathbf{v}_0) d_{v_0}, \tag{47}$$

which has a similar matrix form as equation (45). Thus the non-trivial initial conditions are treated in the same manner as ground accelerations.

4.2 Interval governing equations

To solve the interval differential equation (1), following the DFT approach outlined in Section 3, the equation is transformed into the frequency domain, viz.

$$\left(-\omega_{i}^{2}\mathbf{M}+i\omega_{i}\mathbf{D}+\mathbf{K}\right)\mathcal{F}_{t}(\mathbf{u})_{i}=\mathcal{F}_{t}(\mathbf{f})_{i},\tag{48}$$

where $\mathcal{F}_{t}(\mathbf{u})_{j}$ and $\mathcal{F}_{t}(\mathbf{f})_{j}$ are the Fourier transform of the nodal displacement \mathbf{u}_{k} and equivalent load \mathbf{f}_{k} , respectively.

To include compatibility requirements and essential boundary conditions in the governing equation, and to ensure that the final solution has zero imaginary part, using equations (33) and (34), equation (48) is brought into the following equivalent form,

$$\begin{cases}
\mathbf{K}_{DS,j} & C^T \\
C & 0
\end{cases}
\begin{cases}
\mathcal{F}_i(\mathbf{u})_j \\
\mathcal{F}_i(\lambda)_j
\end{cases} = \begin{cases}
\mathcal{F}_i(\mathbf{f})_j \\
0
\end{cases},$$
(49)

where $\mathbf{K}_{DS,j}$ is the dynamic stiffness matrix corresponding to the *j*-th frequency ω_j , namely

$$\mathbf{K}_{DS,j} = \begin{cases} -\omega_j^2 \mathbf{M} + i\omega_j \mathbf{D} + \mathbf{K}, & 0 \le j < N/2; \\ \text{conjugate of } \mathbf{K}_{DS,N-j}, & N/2 \le j < N, \end{cases}$$
(50)

and C is the constraint matrix that imposes compatibility requirements and essential boundary conditions, and λ_k is the Lagrangian multiplier representing the internal forces and support reactions at t_k . By adopting the Rayleigh damping and the decomposition of **K** and **M** in equation (41), $\mathbf{K}_{DS,j}$ can be decomposed into

$$\mathbf{K}_{DS,i} = A_{DS,i} diag(\Lambda_{DS} \mathbf{\alpha}_{DS}) B_{DS}, \tag{51}$$

where $A_{DS,i}$ is a deterministic matrix depending on the frequency ω_i ,

$$A_{DS,j} = \begin{cases} \{(1+i\beta_d \omega_k) A \ (-\omega_k^2 + i\alpha_d \omega_k) A_m \}, & 0 \le j < N/2; \\ conjugate \ of \ A_{DS,N-j}, & N/2 \le j < N. \end{cases}$$
(52)

and Λ_{DS} , B_{DS} , and α_{DS} are time-invariant variables,

$$\Lambda_{DS} = \begin{cases} \Lambda & 0 \\ 0 & \Lambda_m \end{cases}, \quad B_{DS} = \begin{cases} A^T \\ A_m^T \end{cases}, \quad \boldsymbol{\alpha}_{DS} = \left\{ \boldsymbol{\alpha} \\ \boldsymbol{\alpha}_m \right\}.$$
 (53)

Define

$$\Delta \boldsymbol{\alpha}_{DS} = \boldsymbol{\alpha}_{DS} - \alpha_{DS0},\tag{54}$$

where $\Delta \boldsymbol{\alpha}_{DS}$ is the difference between $\boldsymbol{\alpha}_{DS}$ and the reference deterministic vector $\boldsymbol{\alpha}_{DS0} = \text{mid } (\boldsymbol{\alpha}_{DS})$, and the deterministic dynamic stiffness matrix as

$$K_{DS,i0} = A_{DS,i} diag(\Lambda_{DS} \alpha_{DS0}) B_{DS}. \tag{55}$$

Using the identity

$$A_{DS,j} \operatorname{diag} \left(\Lambda_{DS} \Delta \boldsymbol{\alpha}_{DS} \right) B_{DS} \mathcal{F}_{t}(\mathbf{u})_{j} = A_{DS,j} \left(\Lambda_{DS} \Delta \boldsymbol{\alpha}_{DS} \circ B_{DS} \mathcal{F}_{t}(\mathbf{u})_{j} \right)$$

$$= A_{DS,j} \operatorname{diag} \left(B_{DS} \mathcal{F}_{t}(\mathbf{u})_{j} \right) \Lambda_{DS} \Delta \boldsymbol{\alpha}_{DS},$$
(56)

and given the external load as

$$\mathcal{F}_{t}(\mathbf{f})_{i} = \mathcal{F}_{t}(F\boldsymbol{\delta}\mathbf{d}_{t})_{i} = F\boldsymbol{\delta}\mathcal{F}_{t}(\mathbf{d}_{t})_{i}, \tag{57}$$

then equation (49) takes the following equivalent decomposed form

$$\begin{cases}
K_{DS,j0} & C^{T} \setminus \mathcal{F}_{t}(\mathbf{u})_{j} \\
C & 0 \cdot \mathcal{F}_{t}(\lambda)_{j}
\end{cases} = \begin{cases}
F \\
0
\end{cases} \delta \mathcal{F}_{t}(\mathbf{d}_{t})_{j} - \begin{cases}
A_{DS,j} \\
0
\end{cases} diag(B_{DS}\mathcal{F}_{t}(\mathbf{u})_{j}) \Lambda_{DS} \Delta \boldsymbol{\alpha}_{DS}, \quad (58)$$

However, when the structure is subject to ground motion, according to equation (45), the load vector takes the form

$$\mathcal{F}_{t}(\mathbf{f})_{j} = A_{f} \left(\Lambda_{m} \boldsymbol{\alpha}_{m} \circ B_{f} \boldsymbol{\delta} \right) \mathcal{F}_{t}(\mathbf{d}_{t})_{j}$$

$$= \left(A_{f} \left(\Lambda_{m} \boldsymbol{\alpha}_{m0} \circ B_{f} \boldsymbol{\delta} \right) + A_{f} \left(\Lambda_{m} \Delta \boldsymbol{\alpha}_{m} \circ B_{f} \boldsymbol{\delta} \right) \right) \mathcal{F}_{t}(\mathbf{d}_{t})_{j}$$

$$= F_{0} \boldsymbol{\delta} \mathcal{F}_{t}(\mathbf{d}_{t})_{j} + A_{f} diag \left(B_{f} \boldsymbol{\delta} \mathcal{F}_{t}(\mathbf{d}_{t})_{j} \right) \Lambda_{m} \Delta \boldsymbol{\alpha}_{m},$$
(59)

where $\Delta \alpha_m$ is the difference between α_m and the reference vector α_{m0} , viz. $\Delta \alpha_m = \alpha_m - \alpha_{m0}$, and $F_0 = A_f diag(\Lambda_m \alpha_{m0}) B_f$. Then the generalised equivalent load in equation load in equation (49) is decomposed into

$$\begin{cases}
\mathcal{F}_{t}(\mathbf{f})_{j} \\
0
\end{cases} = \begin{cases}
F_{0} \\
0
\end{cases} \boldsymbol{\delta} \mathcal{F}_{t}(\mathbf{d}_{t})_{j} + \begin{cases}
A_{f} \\
0
\end{cases} diag\left(B_{f} \boldsymbol{\delta} \mathcal{F}_{t}(\mathbf{d}_{t})_{j}\right) \Lambda_{m} \Delta \boldsymbol{\alpha}_{m}, \tag{60}$$

and the equivalent decomposed form of equation (49) becomes

$$\begin{cases}
K_{DS,j0} & C^{T} \\
C & 0
\end{cases}
\begin{cases}
\mathcal{F}_{t}(\mathbf{u})_{j} \\
\mathcal{F}_{t}(\boldsymbol{\lambda})_{j}
\end{cases} = \begin{cases}
F_{0} \\
0
\end{cases} \boldsymbol{\delta} \mathcal{F}_{t}(\mathbf{d}_{t})_{j}$$

$$-\begin{cases}
A_{DS} & A_{f} \\
0 & 0
\end{cases} \operatorname{diag} \begin{cases}
B_{DS} \mathcal{F}_{t}(\mathbf{u})_{j} \\
-B_{f} \boldsymbol{\delta} \mathcal{F}_{t}(\mathbf{d}_{t})_{j}
\end{cases} \right\} \begin{cases}
\Lambda_{DS} \\
0 & \Lambda_{m}
\end{cases} \Delta \boldsymbol{\alpha} DS..$$
(61)

Due to the similarities between the decomposition of the equivalent load in equations (45) and (47), the above formulation can be extended to cases when the initial conditions are non-trivial.

4.3 Iterative enclosure method

To solve the interval linear system of equations (58) and (61), they are recast into the following form

$$K_{\sigma_i} \mathcal{F}_t(\mathbf{u}_{\sigma})_i = F_{\sigma} \delta \mathcal{F}_t(\mathbf{d}_t)_i - A_{\sigma_i} diag(\mathcal{F}_t(\mathbf{v}_{\sigma})_i) \Lambda_{\sigma} \Delta \alpha_{DS}, \tag{62}$$

where $K_{g,j}$, F_g , $A_{g,j}$, Λ_g are given deterministic matrices, \mathbf{u}_g is the unknown interval vector, $\boldsymbol{\delta}$, \mathbf{d}_t , and $\boldsymbol{\Delta}\boldsymbol{\alpha}_{DS}$ are given interval vectors, and \mathbf{v}_g linearly depend on \mathbf{u}_g , viz.

 $\mathbf{v}_g = \mathbf{v}_0 + B_g \mathbf{u}_g$. Here subscripts j denotes variables associated with the j-th frequency ω_j . Note that matrices $K_{g,j}$ and $A_{g,j}$ are functions of the frequency ω_j . In the most general case, \mathbf{u}_g includes \mathbf{u} and $\boldsymbol{\lambda}$, and the auxiliary variable \mathbf{v}_g includes $B_{DS}\mathbf{u}_s - B_f \boldsymbol{\delta} d_f$, and $A_s^T \mathbf{u}_s$.

Now introduce $G_i = K_{g,i}^{-1}$. Multiplying both sides of equation (62) by G_i yields

$$\mathcal{F}_{t}(\mathbf{u}_{g})_{j} = (G_{j}F_{g})\boldsymbol{\delta}\mathcal{F}_{t}(\mathbf{d}_{t})_{j} - (G_{j}A_{g,j})diag(\mathcal{F}_{t}(\mathbf{v}_{g})_{j})\Lambda_{g}\Delta\boldsymbol{\alpha}_{eff}, \tag{63}$$

then

$$\mathbf{u}_{g,k} = (\mathcal{F}_t^{-1}(G_j F_g) * \mathbf{d}_t)_k \delta - (\mathcal{F}_t^{-1}(G_j A_{g,j}) * diag(\mathbf{v}_g))_k \Lambda_g \Delta \boldsymbol{\alpha}_{DS},$$
(64)

where \mathcal{F}_t^{-1} is the IDFT and $(a*b)_k$ denotes the convolution between two discrete signals a_k and b_k , equation (64) can be recast into the following summation form,

$$\mathbf{u}_{g,k} = \left(\sum_{l=0}^{N-1} \mathcal{F}_t^{-1} (G_j F_g)_{k-l} \mathbf{d}_{t,l}\right) \delta - \left(\sum_{l=0}^{N-1} \mathcal{F}_t^{-1} (G_j A_{g,j})_{k-l} diag(\mathbf{v}_{g,l})\right) \Lambda_g \Delta \boldsymbol{\alpha}_{DS}.$$
(65)

Then a fixed-point form for $\mathbf{v}_{g,k}$ is obtained as

$$\mathbf{v}_{g,k} = \mathbf{v}_{0,k} + B_g (\mathcal{F}_t^{-1}(G_j F_g) * \mathbf{d}_t)_k \delta - B_g (\mathcal{F}_t^{-1}(G_j A_{g,j}) * diag(\mathbf{v}_g))_k \Lambda_g \Delta \boldsymbol{\alpha}_{DS}.$$
 (66)

A guaranteed outer enclosure for $\mathbf{v}_{g,k}$ is obtained by iteratively using equation (66), starting from the trivial initial guess $\mathbf{v}_{g,k}^1 = \mathbf{v}_{0,k} + (\mathcal{F}_t^{-1}(G_jF_g)*\mathbf{d}_t)_k \delta$. The iteration stops when no improvement in $\mathbf{v}_{g,k}^j$ is observed for two consecutive iterations, and the converged solution is denoted as $\mathbf{v}_{g,k}^n$. Then the outer solution $\mathbf{u}_{g,k}^{out}$ is obtained by substituting $\mathbf{v}_{g,k}$ in equation (64) with the converged solution $\mathbf{v}_{g,k}^n$.

The convolution between a deterministic signal and an interval signal is computed multiple times, as shown in equations (64) and (66). To increase the computational efficiency and reduce overestimation in the final solution, the FFT-based fast interval convolution algorithm, proposed by Liu and Kreinovich (2010), is adopted. During the iteration in equation (66), only the radius of \mathbf{v}_g is updated, and that will require about 10 iterations for different types and sizes of problems. All other vectors and matrices do not change after the first iteration.

5 Numerical examples

The current IFEM algorithm is implemented using the interval MATLAB toolbox INTLAB (Rump, 990). Interval enclosures of the structural responses of the following sample problems are calculated: (i) a four-storey rigid frame and (ii) a simply supported truss. The performance of the current method is compared against other available methods in the literature: (i) the endpoint combination method (EC) and (ii) the Monte Carlo (MC) simulation. The result shows that the current method is applicable to the transient analysis of structural dynamic problems with uncertain parameters. Guaranteed

interval enclosures of the exact structural responses in the time domain are obtained with small overestimations. In addition, the computational time is negligible when compared with other competing methods.

If deterministic solution is considered as a reference, the run time of interval calculations currently takes 10-15 times the deterministic ones (if interval operations are implemented in the machine hardware, CPU, there will not be any penalty in comparison with floating point calculations), where EC takes 2^n times with n interval parameters, and MC depends on the used number of simulations, 10,000 in the frame example and 100,000 in the truss example.

5.1 Four-storey rigid frame

The first example is a four-storey frame shown in Figure 3. The floors of the frame are assumed to be rigid enough to model the structure as an equivalent spring-mass system (shown in the right-hand side of Figure 3). The mass \mathbf{m}_j and the inter-storey shear stiffness \mathbf{k}_j of each floor ($j=1,\ldots,4$) are modelled by independent interval variables, and given in Table 1.

Figure 3 A four-storey rigid frame and the equivalent spring-mass system

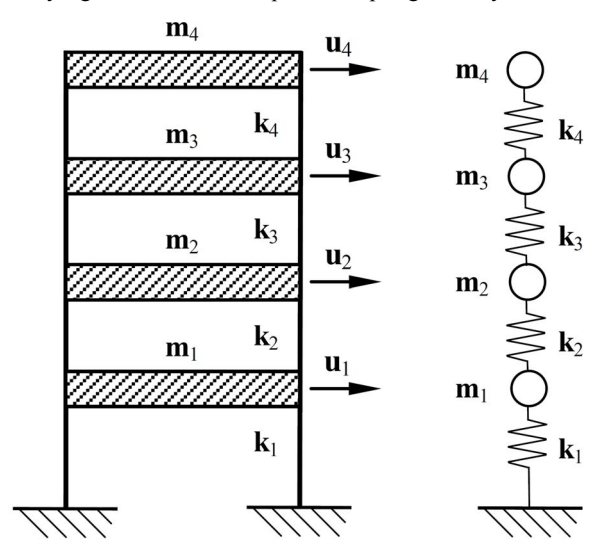


Table 1 Interval mass and stiffness for the five-storey rigid frame of Figure 3, including 1% uncertainties in mass, and 5% uncertainties in stiffness

Floor	Mass (kg)			Stiffness (kN/m)		
	\mathbf{m}_{j}	$mid \mathbf{m}_j$	$rad \mathbf{m}_{j}$	\mathbf{k}_{j}	$mid \mathbf{k}_{j}$	$rad \mathbf{k}_{j}$
1	[5.416, 5.470]	5.443	0.027	[1.180, 1.240]	1.210	0.030
2	[5.416, 5.470]	5.443	0.027	[1.677, 1.763]	1.720	0.043
3	[5.416, 5.470]	5.443	0.027	[1.862, 1.958]	1.910	0.048
4	[5.416, 5.470]	5.443	0.027	[1.775, 1.865]	1.820	0.045

Consider the structural response of the frame under a concentrated impact force acting on the top floor. The force has a duration of 4 s, and its variation during that time is deterministic, viz.

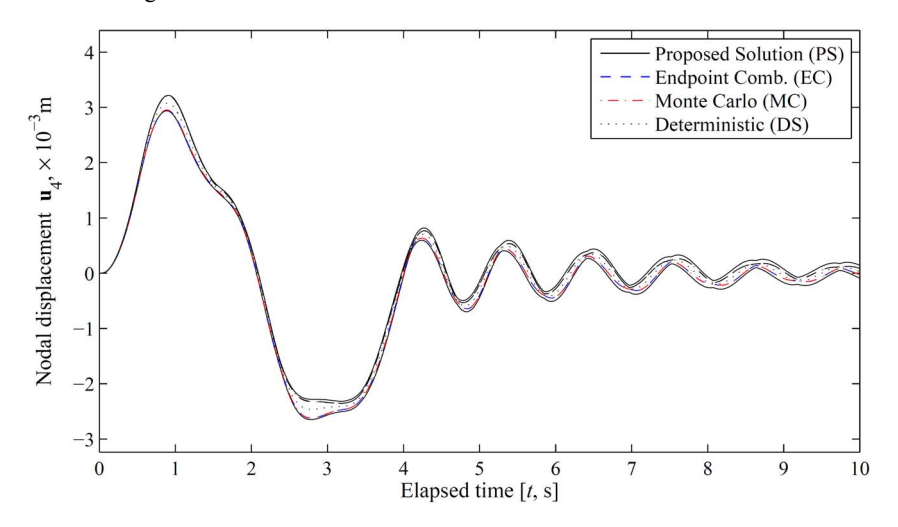
$$\mathbf{f}(t) = \begin{cases} \mathbf{P}\sin(\pi t/2), & 0 \le t \le 4 \,\mathrm{s}; \\ 0, & t > 4 \,\mathrm{s}, \end{cases}$$

$$\tag{67}$$

where $\mathbf{P} = [0.99, 1.01]$ kN (2% uncertainty in the magnitude of the load). The damping matrix $\mathbf{D} = 0.5\mathbf{M} + 5 \times 10^{-3}\mathbf{K}$. The sampling rate is 100 Hz, so the sampling interval $\Delta t = 0.01$ s.

Figure 4 compares the lower and upper bounds of \mathbf{u}_4 for the first 10 s, obtained from the current Proposed Solution (PS, black solid lines), Monte Carlo predictions (MC, red dashed-dotted lines) from an ensemble of 10,000 simulations, the reference solution obtained from endpoint combination (EC, blue dash lines), and the deterministic solution (DS, black dotted line). Note that PS always contains the reference solution EC, and MC is always contained by EC. In addition, the overestimation level of the current method slightly increases as the time increases. The MC solution is obtained using the DFT approach, which indistinguishable from the solution obtained from a recursive Newmark- β method.

Figure 4 Lower and upper bounds of the nodal displacement **u**₄ for the four-storey frame of Figure 3 under a sinusoidal force. MC from an ensemble of 10,000 simulations. Material uncertainty is 1% for mass, and 5% for stiffness. Load uncertainty is 2% for the magnitude



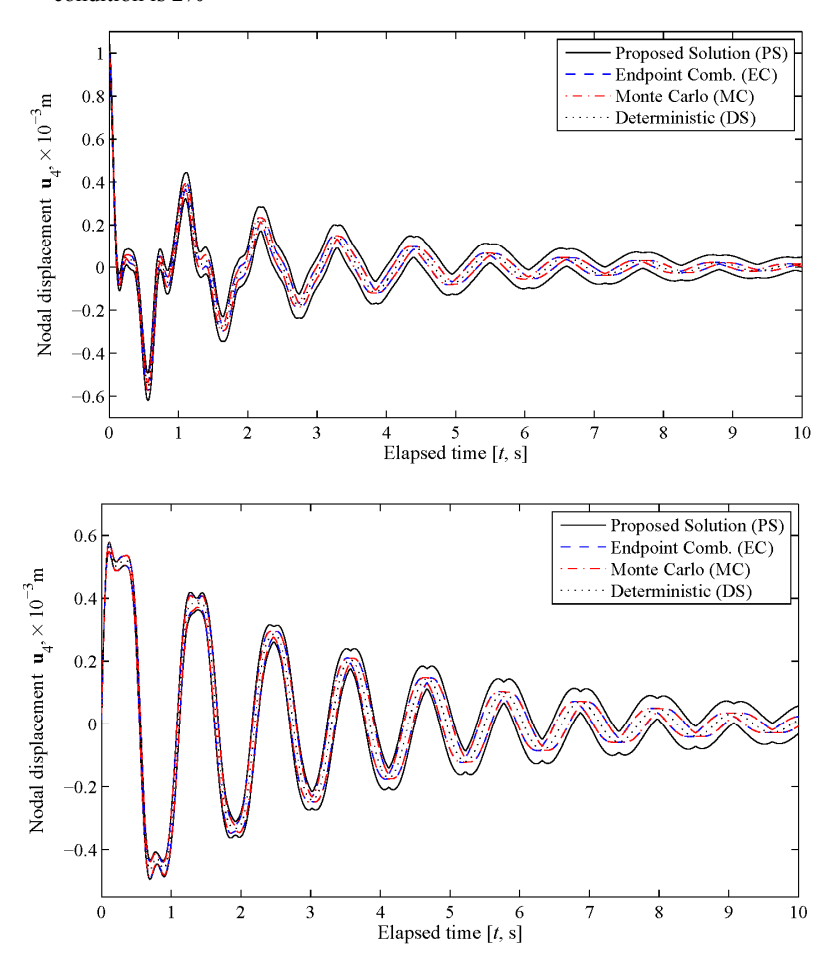
Then the concentrated force $\mathbf{f}(t)$ is removed, and the structure is subject to non-trivial initial conditions. Figure 5 shows the nodal displacement \mathbf{u}_4 at the top floor for the first

10 s with non-trivial initial nodal displacement \mathbf{u}_0 (top) and nodal velocity \mathbf{v}_0 (bottom), respectively. Here 2% uncertainty is considered for \mathbf{u}_0 and \mathbf{v}_0 , viz.

$$\mathbf{u}_0 = \{0 \ 0 \ 0 \ 0 \ [0.99, \ 1.01]\}^T \times 10^{-3} \,\mathrm{m}; \mathbf{v}_0 = \{0 \ 0 \ 0 \ 0 \ [0.99, \ 1.01]\}^T \times 10^{-2} \,\mathrm{m/s}.$$
(68)

Figure 5 shows that the high frequency components dissipate quickly. After about 3 s, the response of the structure is dominated by the lowest frequency vibration. Observe that the performance of the current method is the same as in the previous case. The obtained interval solution guarantees to enclose the reference solution (endpoint combination, EC), and the overestimation level increases slightly as the time increases. Thus non-trivial initial conditions are handled successfully.

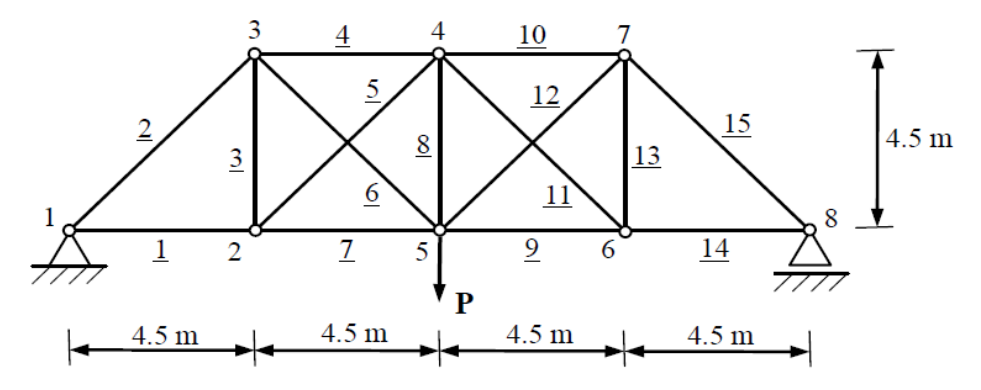
Figure 5 Lower and upper bounds of the nodal displacement ${\bf u}_4$ for the four-storey frame of Figure 3 under non-trivial initial conditions: (top) non-trivial initial displacement ${\bf u}_0$, (bottom) non-trivial initial velocity ${\bf v}_0$. MC from an ensemble of 10,000 simulations. Material uncertainty is 1% for mass, and 5% for stiffness. Uncertainty in the initial condition is 2%



5.2 Simply supported truss

The second example is a simply supported symmetric truss composed of 15 bars, as shown in Figure 6. The joints are labelled from 1 to 8, and the bars are labelled from 1 to 15. Time-varying concentrated load **P** acts at joint 5. Bars 1 to 3, 13 to 15 have the same cross section area $A = 1.0 \times 10^{-3} \,\mathrm{m}^2$, and all other bars, viz. bars 4 to 12, have smaller cross section area $A = 6.0 \times 10^{-4} \,\mathrm{m}^2$. All the bars are made of steel. They have the interval mass density ρ with midpoint value $\rho = 7.8 \times 10^3 \,\mathrm{kg/m}^3$, and the interval Young's modulus **E** with midpoint value $E = 200 \,\mathrm{GPa}$.

Figure 6 A simply supported symmetric truss subject to concentrated force



Fifteen bar elements are used to model the truss in Figure 6. Element mass density ρ and Young's modulus **E** are assumed independent, and they are modelled by 30 interval variables. The midpoint of the load **P** is a sinusoid with a frequency of 50 Hz and an amplitude of 200 kN, viz.

$$P = 200\sin(100\pi t) \text{ kN}. \tag{69}$$

The damping matrix $\mathbf{D} = 20\mathbf{M} + 3 \times 10^{-5} \mathbf{K}$. The sampling rate is 10 kHz, so $\Delta t = 1 \times 10^{-4}$ s. Then vertical displacement \mathbf{v}_5 at joint 5 is selected for comparison among the various methods mentioned previously. Consider 10% uncertainty for the load magnitude and 1% for the load time-history, as well as Young's modulus and mass density of each bar. Figure 7 plots the lower and upper bounds of \mathbf{v}_5 for the first 0.1 s obtained from the proposed current solution (PS, solid lines) and the Monte Carlo predictions (MC, dashed lines from the Newmark- β approach, and dash-dotted lines from the DFT approach) from an ensemble of 100,000 simulations. Observe that the current method obtains guaranteed enclosures of the MC prediction.

Figure 7 Lower and upper bounds of the nodal displacement \mathbf{v}_5 at joint 5 for the truss of Figure 6 under external loads. MC predictions (Newmark- β and DFT) from an ensemble of 100,000 simulations. Parameter uncertainties are 10% for load magnitude, 1% for load history, Young's modulus, and mass density

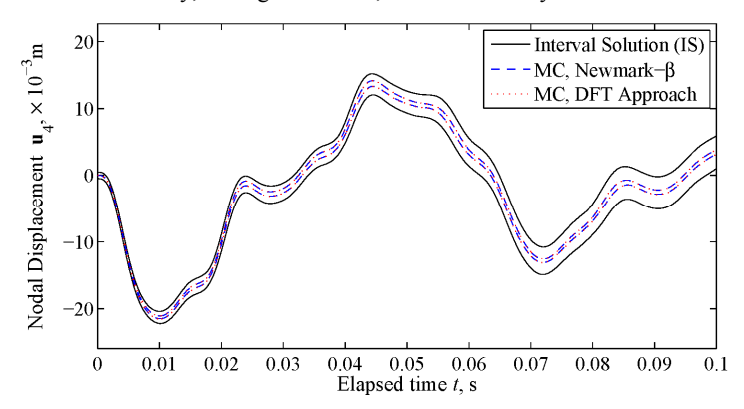


Figure 8 Lower and upper bounds of the nodal displacement v₅ at joint 5 of the truss of Figure 6 with: (top) 2% uncertainty only in load history; (bottom) 20% uncertainty in load magnitude, 1% uncertainties in Young's modulus and mass density. MC predictions (Newmark-β: and DFT from an ensemble of 100,000 simulations)

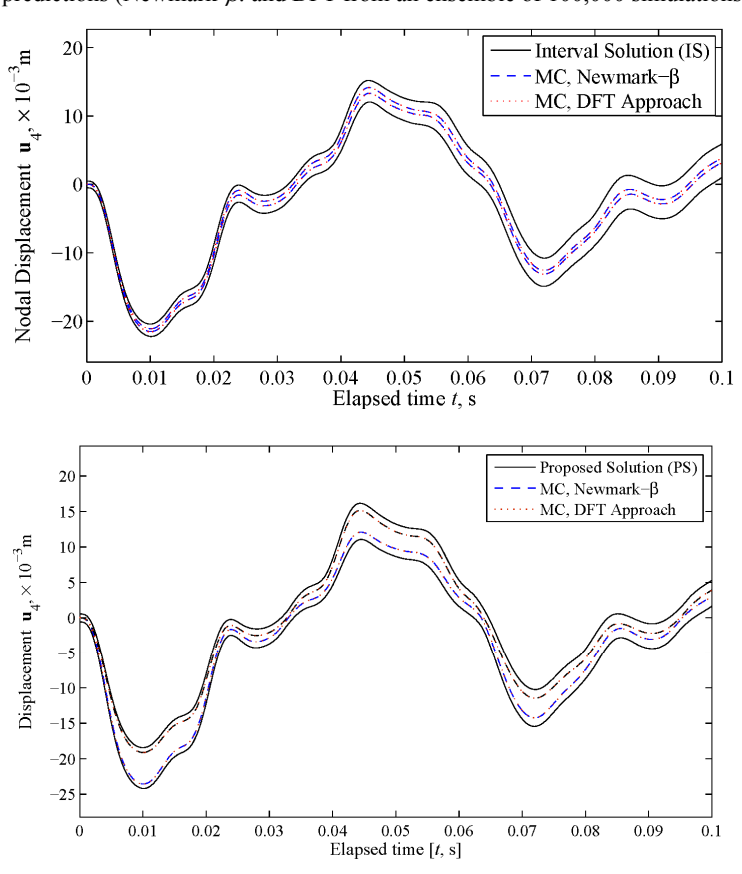


Figure 7 shows that the uncertainties in the structural responses increase significantly over time. This behaviour is due to the fact that the load history uncertainties are modelled by independently varied intervals at different time steps. In the current example, this means 0.1 s × 10 kHz = 1000 independent interval variables. As a result, the overall uncertainty level is much higher than 1%. This also explains the growing differences between PS and MC predictions over time. Figure 8 considers (top) 2% uncertainties in load time-history, (bottom) 20% uncertainties in load magnitude, and 1% Young's modulus, and mass density. Observe that in the bottom subplot, the uncertainties now do not increase over time, and the difference between PS and MC is much smaller than the top subplot. So it is indeed the increased number of interval variables that caused the increased uncertainty and the difference between PS and MC.

6 Conclusion

We present a new spectral-based interval finite element formulation for the time-domain dynamic analysis of elastic structures with uncertain load, geometric, and material properties. Ground motion and non-trivial initial conditions are successfully handled, resulting in a method that is both efficient and widely applicable.

Uncertain parameters of the structure are modelled as intervals. The interval enclosures guarantee to enclose the exact solution set with small overestimation, even for large uncertainty levels. Numerical examples show that the proposed method gives guaranteed sharp bounds on the dynamic structural responses in comparison to other methods that give over-optimistic predictions on lower and upper bounds.

References

- Adhikari, S. and Khodaparast, H.H. (2014) 'A spectral approach for fuzzy uncertainty propagation in finite element analysis', *Fuzzy Sets and Systems*, Vol. 243, pp.1–24.
- Alefeld, G. and Herzberger, J. (1984) Introduction to Interval Computation, Academic Press.
- Bae, S.H., Cho, J.R., Bae, S.R. and Jeong, W.B. (2014) 'A discrete convolutional Hilbert transform with the consistent imaginary initial conditions for the time-domain analysis of five-layered viscoelastic sandwich beam', *Computer Methods in Applied Mechanics and Engineering*, Vol. 268, pp.245–263.
- Bai, Y.C., Jiang, C., Han, X. and Hu, D. A. (2013) 'Evidence-theory-based structural static and dynamic response analysis under epistemic uncertainties', Finite Elements in Analysis and Design, Vol. 68, pp.52–62.
- Corliss, G., Foley, C. and Kearfott, R. B. (2007) 'Formulation for reliable analysis of structural frames', *Reliable Computing*, Vol. 13, No. 2, pp.125–147.
- De Borst, R., Crisfield, M. A., Remmers, J.J.C. and Verhoosel, C.V. (2012) *Nonlinear Finite Element Analysis of Solids and Structures*, John Wiley & Sons.
- Dehghan, M., Hashemi, B. and Ghatee, M. (2006) 'Computational methods for solving fully fuzzy linear systems', *Applied Mathematics and Computation*, Vol. 179, No. 1, pp.328–343.
- Dempster, A.P. (1967) 'Upper and lower probabilities induced by a multi-valued mapping', *The Annals of Mathematical Statistics*, Vol. 38, pp.325–339.
- Do, D.M., Gao, W., Song, C. and Tangaramvong, S. (2014) 'Dynamic analysis and reliability assessment of structures with uncertain-but-bounded parameters under stochastic process excitations', *Reliability Engineering & System Safety*, Vol. 132, pp.46–59.

- Dokainish, M.A. and Subbaraj, K. (1989) 'A survey of direct time-integration methods in computational structural dynamics: I. Explicit methods', *Computers & Structures*, Vol. 32, No. 6, pp.1371–1386.
- Erdogan, Y.S. and Bakir, P.G. (2013) 'Inverse propagation of uncertainties in finite element model updating through use of fuzzy arithmetic', *Engineering Applications of Artificial Intelligence*, Vol. 26, No. 1, pp.357–367.
- Fernández-Martnez, J.L., Fernández-Muñiz, Z., Pallero, J.L.G. and Pedruelo-González, L.M. (2013) 'From Bayes to Tarantola: new insights to understand uncertainty in inverse problems', *Journal of Applied Geophysics*, Vol. 98, pp.62–72.
- Gao, W. (2007) 'Natural frequency and mode shape analysis of structures with uncertainty', Mechanical Systems and Signal Processing, Vol. 21, No. 1, pp.24–39.
- Hu, J. and Qiu, Z. (2010) 'Non-probabilistic convex models and interval analysis method for dynamic response of a beam with bounded uncertainty', *Applied Mathematical Modelling*, Vol. 34, No. 3, pp.725–734.
- Igusa, T., Buonopane, S.G. and Ellingwood, B.R. (2002) 'Bayesian analysis of uncertainty for structural engineering applications', *Structural Safety*, Vol. 24, No. 2, pp.165–186.
- Impollonia, N. (2006) 'A method to derive approximate explicit solutions for structural mechanics problems', *International journal of solids and structures*, Vol. 43, No. 22, pp.7082–7098.
- Impollonia, N. and Muscolino, G. (2011) 'Interval analysis of structures with uncertain-but-bounded axial stiffness', *Computer Methods in Applied Mechanics and Engineering*, Vol. 200, No. 21, pp.1945–1962.
- Jiang, C., Zhang, Z., Han, X. and Liu, J. (2013) 'A novel evidence-theory-based reliability analysis method for structures with epistemic uncertainty', *Computers & Structures*, Vol. 129, pp.1–12, 2013.
- Klir, G.J. and Wierman, M.J. (1999) Uncertainty-Based Information Elements of Generalized Information Theory, Physica-Verlag, Heidelberg.
- Kulisch, U.W. and Miranker, W. L. (1981) Computer Arithmetic in Theory and Practice, Academic Press, New York.
- Lee, U., Kim, S. and Cho, J. (2005) 'Dynamic analysis of the linear discrete dynamic systems subjected to the initial conditions by using an FFT-based spectral analysis method', *Journal of Sound and Vibration*, Vol. 288, No. 1, pp.293–306.
- Liu, F., Li, H., Wang, W. and Liang, B. (2015) 'Initial-condition consideration by transferring and loading reconstruction for the dynamic analysis of linear structures in the frequency domain', *Journal of Sound and Vibration*, Vol. 336, pp.164–178.
- Liu, G. and Kreinovich, V. (2010) 'Fast convolution and fast Fourier transform under interval and fuzzy uncertainty', *Journal of Computer and System Sciences*, Vol. 76, No. 1, pp.63–76.
- Lutes, L.D. and Sarkani, S. (2004) Random Vibrations: Analysis of Structural and Mechanical Systems, Butterworth-Heinemann.
- Mansur, W.J., Carrer, J.A.M., Ferreira, W.G., Claret, D.G.A. and Venancio-Filho, F. (2000) 'Time-segmented frequency-domain analysis for non-linear multi-degree-of-freedom structural systems', *Journal of Sound and Vibration*, Vol. 237, No. 3, pp.457–475.
- Moens, D. and Hanss, M. (2011) 'Non-probabilistic finite element analysis for parametric uncertainty treatment in applied mechanics: recent advances', *Finite Elements in Analysis and Design*, Vol. 47, No. 1, pp.4–16.
- Moore, R.E., Kearfott, R.B. and Cloud, M.J. (2009) *Introduction to Interval Analysis*, Society for Industrial and Applied Mathematics.
- Muhanna, R.L. and Mullen, R.L. (2001) 'Uncertainty in mechanics problems-interval-based approach', *Journal of Engineering Mechanics*, American Society of Civil Engineers, Vol. 127, No. 6, pp.557–566.
- Muhanna, R.L., Zhang, H. and Mullen, R.L. (2007) 'Combined axial and bending stiffness in interval finite-element methods', *Journal of Structural Engineering*, Vol. 133, No. 12, pp.1700–1709.

- Mullen, R.L. and Muhanna, R.L. (1999) 'Bounds of structural response for all possible loading combinations', *Journal of Structural Engineering*, Vol. 125, No. 1, pp.98–106.
- Neumaier, A. and Pownuk, A. (2007) 'Linear systems with large uncertainties, with applications to truss structures', *Reliable Computing*, Vol. 13, No. 2, pp.149–172.
- Paz, M. (1997) Structural Dynamics: Theory and Computation, Springer Science & Business Media.
- Qiu, Z. and Ni, Z. (2010) 'An inequality model for solving interval dynamic response of structures with uncertain-but-bounded parameters', *Applied Mathematical Modelling*, Vol. 34, No. 8, pp.2166–2177.
- Rama Rao, M.V., Mullen, R.L. and Muhanna, R.L. (2011) 'A new interval finite element formulation with the same accuracy in primary and derived variables', *International Journal of Reliability and Safety*, Vol. 5, No. 3, pp.336–357.
- Rump, S.M. (1999) INTLAB INTerval LABoratory, Kluwer Academic Publishers, pp.77–104.
- Santamarina, J.C. and Fratta, D. (2005) Discrete Signals and Inverse Problems: an Introduction for Engineers and Scientists, John Wiley & Sons.
- Shafer, G. (1968) A Mathematical Theory of Evidence, Princeton University Press, Princeton.
- Soize, C. (2013) 'Bayesian posteriors of uncertainty quantification in computational structural dynamics for low-and medium-frequency ranges', *Computers & Structures*, Vol. 126, pp.41–55.
- To, C. and Solomon, W. (2012) 'Response analysis of nonlinear multi-degree-of-freedom systems with uncertain properties to non-Gaussian random excitations', *Probabilistic Engineering*, Vol. 27, No. 1, pp.75–81.
- Unger, J.F. and Könke, C. (2011) 'An inverse parameter identification procedure assessing the quality of the estimates using Bayesian neural networks', *Applied Soft Computing*, Vol. 11, No. 4, pp.3357–3367.
- Veletsos, A.S. and Kumar, A. (1983) 'Steady-state and transient responses of linear structures', Journal of Engineering Mechanics, American Society of Civil Engineers, Vol. 109, No. 5, pp.1215–1230.
- Veletsos, A.S. and Ventura, C.E. (1985) 'Dynamic analysis of structures by the DFT method', *Journal of Structural Engineering*, American Society of Civil Engineers, Vol. 111, No. 12, pp.2625–2642.
- Xia, Y., Qiu, Z. and Friswell, M.I. (2010) 'The time response of structures with bounded parameters and interval initial conditions', *Journal of Sound and Vibration*, Vol. 329, No. 3, pp.353–365.
- Xiao, N. (2015) Interval finite element approach for inverse problem under uncertainty, PhD Thesis, Georgia Institute of Technology.
- Yang, Y., Cai, Z. and Liu, Y. (2012) 'Interval analysis of dynamic response of structures using Laplace transform', *Probabilistic Engineering Mechanics*, Vol. 29, pp.32–39.
- Zhang, H. (2005) Nondeterministic Linear Static Finite Element Analysis: an Interval Approach, PhD Thesis, Georgia Institute of Technology.